SAND2012-7294C

Impact of Aperture Size, Receiver Diameter, and Loop Length on Parabolic Trough Performance with Consideration of Heat Loss, Pumping Parasitics, and Optics for a Typical Meteorological Year

Kyle W. Glenn[1] and Clifford K. Ho[2]

[1]Sandia National Laboratories, Concentrating Solar Technologies Department, P.O. Box 5800, Albuquerque, NM 87185-1127, USA, (575) 635-6248, kglenn@sandia.gov

[2]Ph.D., Sandia National Laboratories, Concentrating Solar Technologies Department, P.O. Box 5800, Albuquerque, NM 87185-1127, USA, (505) 844-2384, ckho@sandia.gov

1. Introduction

Recent studies have suggested that changing the geometry of the current 5 meter parabolic troughs may increase their collection efficiency. One such change is doubling the aperture size to 10 m [1]. The benefit of this change would be an increase in the thermal energy collected per square meter of collector area without a proportional increase in heat loss. This would cause a net gain in energy collected per square meter. However, increasing the aperture size impacts several aspects of trough performance. Optically, the distance a beam must travel from the collector to the receiver will increase. Consequently, the reflected beams' angular width increases and may not be wholly encompassed by the receiver tube, resulting in the loss of thermal energy. Also, increasing the aperture size will require that the velocity of the heat transfer fluid (HTF) flow be increased to maintain the trough loop's outlet temperature if the loop length is held constant [2]. The pressure drop within the HTF and the parasitic pumping requirement will increase. These effects can be remedied by increasing the receiver tube diameter. However, a larger receiver tube will cause an increase in heat loss because of its increased convective surface area [2].

The trade-offs mentioned above prompted this study which investigates the annual performance of parabolic troughs, particularly heat losses, optical losses, and parasitic pressure drop while varying the loop length, aperture size, and receiver size of a parabolic trough. A Matlab model was created to determine the trough field performance on an annual basis. It calculated the heat losses, parasitic pressure drop, and optical losses and converted these quantities into an equivalent quantity of electrical energy using a presumed thermal-to-electric efficiency of a trough plant and pumping power curves. The trough fields were judged based on how much net annual electrical energy was captured. This quantity is determined by deducting the annual parasitic pumping electrical energy required for energy collection from the equivalent electrical energy captured by the troughs. The energy required to rotate the troughs about their focal axis to stay on sun is negligible [3]. The study showed that a trough that had a 6 m aperture, 7 cm receiver tube, and 200 m loop length collected the most net electrical energy annually (116.6 GWh_e). A 10 m trough with a 14 cm receiver tube collected the most net electrical energy annually at the current SEGS VI loop length of approximately 750 meters.

2. Approach

To perform the annual analysis a Matlab model was created to calculate the performance of parabolic trough power plants with varying trough configurations. Annual data was taken from a Typical Meteorological Year (TMY) data set for Daggett, CA, particularly TMY2, which contains hourly values of solar radiation and meteorological data that is "typical" for a region based on a 30-year period (TMY2 covers 1961-1990) [4]. The TMY2 data, particularly the values for the direct normal irradiance were used to determine the flux on the receiver.

The flux added to the receiver is determined by the Matlab model in several steps. First, the model determines the position of the sun relative to a parabolic trough's focal axis in terms of an angular offset from the focal plane termed the incidence angle. The incidence angle determines the distance that all beams

reflected from the collector must travel before being intercepted by the receiver tube, and the associated beam spread is determined. The parabola shape is given in Equation (1 and is a function of the focal length. In this analysis, when the aperture size is varied the focal length to aperture size ratio remains the same.

$$y(x) = \frac{1}{4 * FL} * x^2 \tag{1}$$

where $FL =$ focal length (m).

Using the equation for the parabola shape and the incidence angle the distance from the collector to the receiver can be determined as shown in Equation (2.

$$D_{focus} = \frac{x}{\sin\left(tan^{-1}\left(x * \frac{cos(\theta_{inc})}{FL - y(x)}\right)\right)} \tag{2}$$

Where. $\theta_{inc} =$ incidence angle (mrad).

Half of the angular width of the receiver tube at the location where a reflected ray intersects the receiver can be found using Equation (3.

$$\theta_x = \tan^{-1}\left(\frac{0.5D_3}{D_{focus}(x)}\right) \tag{3}$$

where, $D_3 =$ outer diameter of absorber tube (m).

The portion of the beam width that is occupied by the receiver tube and the flux that exists in this region was determined based on a functional relationship that was created for the flux distribution within the sun's subtended angle (Equation (4); this equation was found using a process of trial and error.

$$Flux(\theta) = \frac{1 - 0.013 * \theta^2}{\frac{10 * \cosh(5\theta)}{e^{23}} + 1} \tag{4}$$

where, $\theta =$ subtended angle (mrad).

Equation (4 is plotted against data from Rabl and Bendt [5] and the data used in the Circe and Helios softwares [6] in Figure 1. Equation (4 satisfactorily matches the data.

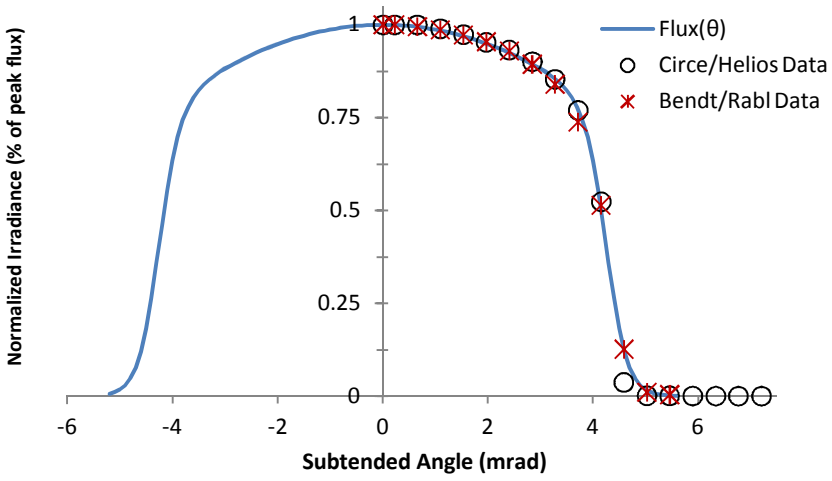

Figure 1. Plot comparing data from Rabl and Bendt [5] and the data used in Circe and Helios [6] again against a functional relationship for the sun's flux within its subtended angle.

For convenience Equation (4 was normalized based on the total flux under the curve, rather than the peak flux. Therefore, the area under the flux distribution curve was equal to 1, simplifying subsequent calculations. The normalization was done by multiplying Equation (4 by the inverse of the area under the curve (Equation

(5).

$$C = \frac{1}{2 * \int_0^{4.65} \text{Flux}(\theta) d\theta} = .1278 \tag{5}$$

Equation (4 can also be manipulated to represent the flux distribution for beams reflected from surfaces with various RMS slope errors. The relation in Equation (6 when coupled with the factors K and J of Equations (7 and (8, respectively, relates the angular width of the flux distribution to the RMS slope error of a reflective surface. These equations were found through a process of trial and error by comparing intercept factors calculated by the Matlab model and SolTrace, a ray tracing software from the National Renewable Energy Laboratory [7].

$$f(\sigma_{RMS}) = 4.65 + J * \sigma_{RMS}^{K} \tag{6}$$

$$K = (9.6 * 10^{-5} * \theta_{inc} - 2.2 * 10^{-7} * \theta_{inc}^2) * [(CR - 142.85714) + .99] \tag{7}$$

$$\begin{aligned} J = \left(1.8^{\frac{110}{CR*8.5}} + .91\right) \\ * [(2.32 * 10^{-4} * \theta_{inc} + 8.1 * 10^{-7} * \theta_{inc}^2) * CR \\ + (3.49 * 10^{-2} * \theta_{inc} - 2.5 * 10^{-4} * \theta_{inc}^2 + 1)] \\ + \left[\frac{1}{1.5^{(-\theta_{inc}+43.5)} + 1} * (6 * 10^{-5} * (CR - 93)^2 - .07)\right] \end{aligned} \tag{8}$$

where, $\sigma_{RMS} = \text{RMS slope error}$, and $CR = DA/DR$.

The ratio of the original angular width to that of the widened beam is given in Equation (9.

$$W(\sigma_{\text{RMS}}) = \frac{4.65}{f(\sigma_{\text{RMS}})} \tag{9}$$

By multiplying every instance of "θ" in Equation (4 by the width ratio of Equation (9, the flux distribution will be stretched to the angular width specified by Equation (6. Multiplying the resulting equation again by the width ratio will decrease the amplitude of the function. Doing so will ensure that the total area under the flux distribution curve will be preserved after stretching. This stretching and shrinking maintains the sun's shape; it does not distort it. Equation (10 (hereto referred to as the modified flux distribution) is the result of normalizing the total area under the flux distribution of Equation (4 to be equal to 1, and to manipulate it to model a widened beam while preserving the quantity of flux after it has been reflected from a surface with varying RMS slope errors.

$$Flux_{total\ normalized}(\theta, \sigma_{\text{RMS}}) = C * W(\sigma_{\text{RMS}}) * \left(\frac{1 - 0.013 * [W(\sigma_{\text{RMS}}) * \theta]^2}{\frac{10 * \cosh(5[W(\sigma_{\text{RMS}}) * \theta])}{e^{23}} + 1} \right) \tag{10}$$

The amount of flux present in the region of a reflected beam that is occupied by the receiver can be determined by integrating the modified flux distribution over the angular width of the receiver found in Equation (3. This power incident on the receiver is integrated over the collector, and the ratio of the power intercepted to the power incident on the collector is the intercept factor (Equation (11).

$$IF = \cos(\theta_{inc}) * 4 \int_0^{0.5DA} \int_0^{\theta_x(x)} Flux_{total\ normalized}(\theta, \sigma_{\text{RMS}}) d\theta dx \tag{11}$$

Where, $DA = \text{aperture width}$.

Intercept factors calculated by the Matlab model using Equation (11 have been plotted against those found by SolTrace in Figure 2.

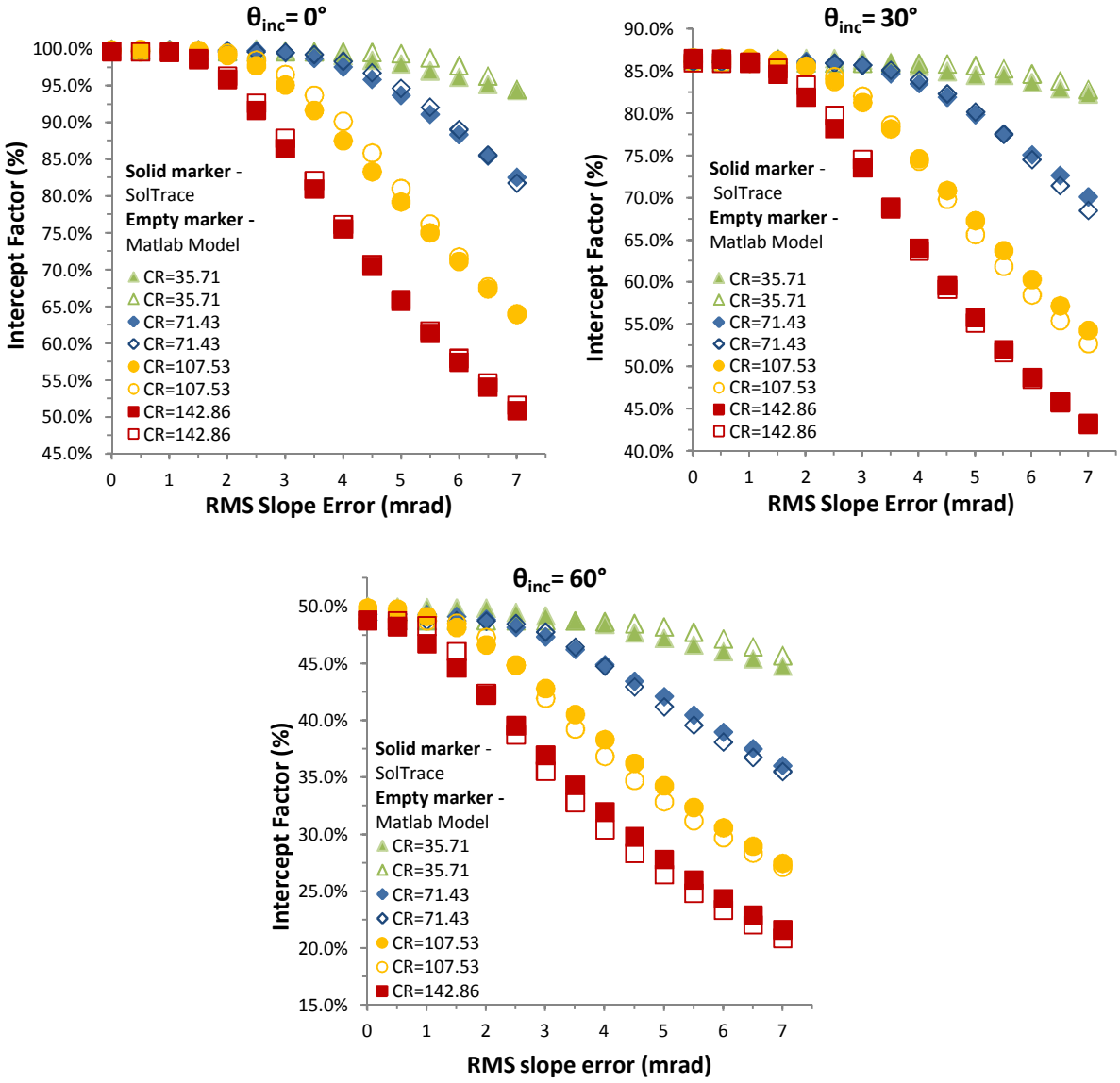

Figure 2. Plots comparing intercept factors calculated by the Matlab model and SolTrace for representative concentrations ratios and incidence angles as a function of RMS slope error.

Overall, there were 300 SolTrace simulations with which Matlab was compared to (not all are shown). When equations (6 through (8 are used for the beam spreading, Matlab and SolTrace differ by 2% or less. There are a few instances where they differ by more than 2%, but this occurs in less than 5% of the data and only reaches as high as 2.6%. Note that this correlation is valid for concentration ratios between 35.71 and 142.86 (half double of the base case), incidence angles between 0 and 60 degrees, and slope errors ranging from 0 to 7 mrad. While the correlation between Matlab and SolTrace was not exhaustively evaluated, it was checked across a broad range of incidence angles, concentration ratios, and slope errors within the limits just mentioned and matched well. Also, this relation only applies concentration ratios whose focal length to aperture size ratio is the same as the base case.

The hourly value of the direct normal irradiance (DNI) taken from the TMY data is multiplied by the intercept factor and aperture width to determine the flux added to the receiver (Equation (12).

$$Q_{in} = IF * DNI * DA \tag{12}$$

Now that the flux on the receiver is known the thermal performance of each prescribed trough loop

configuration is calculated in increments of 2.5 meters using the Forristall model [8], a radial resistive network describing the heat transfer characteristic of the heat collecting element (HCE) shown in Figure 3, hereto referred to as the receiver. The thermal energy absorbed by the HTF and the thermal energy lost to the environment per unit length are determined using this model based on the flux added to the receiver from the collector that was determined in Equation (12.

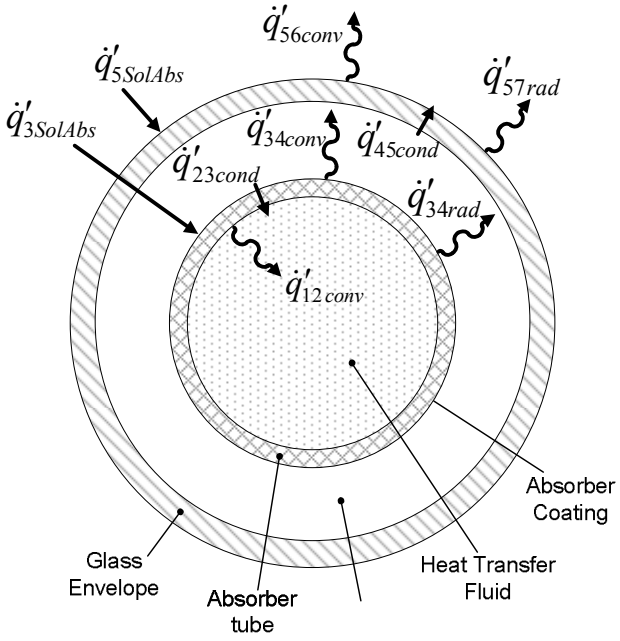

Figure 3. Cross Section Illustrating the Components of an HCE and the Heat Transfer Modes that Describe the Flow of Thermal Energy

Using the thermal energy absorbed by the HTF, particularly $\dot{q}'_{12conv}$, the energy added to each 2.5 meter long element can be determined (Equation (13)).

$$\dot{Q}_{cv} = \dot{q}'_{12conv} * Element\ Length \tag{13}$$

A control volume analysis was performed on each element (Equation (14) to determine the outlet conditions with which to evaluate a subsequent element. Elements were added until the desired outlet conditions were reached. Restrictions on the mass flow rate were imposed to prevent the plant from operating when the DNI did not have the intensity necessary for the loop to reach the desired outlet temperature without going below 1/7 of the design flow rate. Also, the minimum mass flow rate would be adjusted to a higher quantity to avoid a laminar flow. However, this condition was not encountered in the analysis. The maximum mass flow rate could never exceed what the plant's HTF pump could provide and was adjusted to a lower quantity if the pressure at the loop inlet exceeded what the HCE could contain.

$$\dot{Q}_{cv} = \dot{m}\left[\int_{T1}^{T2} C_p(T)\,dT + \frac{1}{2}\left(\frac{\dot{m}}{\rho_{@T2}\,A}\right)^2 - \frac{1}{2}\left(\frac{\dot{m}}{\rho_{@T1}\,A}\right)^2\right] \tag{14}$$

where, $\rho =$ density of HTF, $C_p =$ specific heat of HTF, $\dot{m} =$ mass flow rate, $A =$ cross section area, $T_2 =$ element HTF inlet temperature, and $T_2 =$ element HTF outlet temperature.

After a loop has been modeled the pressure drop across the loop can be found with Equation (15 [2].

$$\Delta P = \left(0.184 * Re_D^{-\frac{1}{5}} * l_{pipe} + n_{joints} F_{joint}\right)\frac{\rho V^2}{2D_2} \tag{15}$$

where,$Re_D =$ Reynold's Number,$l_{pipe} =$ length of absorber pipe,$n_{joints} =$ number of connective joints, $F_{joint} =$ friction factor of connective joint, and $V =$velocity of HTF flow.

The hourly values of the thermal energy captured by all the receiver elements in a loop and the pressure drop are summed and multiplied by the number of loops in the collector field. This field-wide thermal energy collected ($\dot{Q}_{Field}$) is converted into electrical energy by multiplying it by an assumed thermal-to-electric efficiency (0.378) of the power block (Equation (16).

$$\dot{E}_{QG} = 0.378 * \dot{Q}_{Field} \tag{16}$$

The field-wide parasitic pressure drop is also converted to electrical energy with Equation (17.

$$\dot{E}_{PD} = \frac{\dot{m}\,\Delta P}{\rho\,\eta_{pump}\,\eta_{motor}\,\eta_{varsp}} \tag{17}$$

where, $\eta_{pump} = 0.80$, $\eta_{motor} = 0.95$, and $\eta_{varsp} = 0.95$ [9].

The SEGS VI trough plant was used as the reference case to be populated with a collector field consisting of parabolic troughs with varying aperture sizes, receiver diameters, and loop lengths. The thermal performance and pressure drop were calculated on an hourly basis for all of TMY2. Look up tables and numerical integrations were used extensively.

3. Results and Discussion

The Matlab model calculated the annual performance of trough configurations with aperture sizes varying from 5 m to 10 m while the receiver diameter was varied from 7 cm to 14 cm. Loop lengths ranging from 200 m to 1300 m were evaluated at increments of 100 m. The gray dashed lines in Figures 4 through 6 mark the current SEGS VI loop length. Each trough configuration is evaluated at an RMS slope error of 5.4 and 2.5 mrad. The 5.4 mrad RMS slope error is based on the current slope error budget with which 5 m troughs are evaluated [1]. An RMS slope error of 2.5 mrad is required for a 2× trough which has a 10 m aperture to have the same optical performance as a 5 m trough. For convenience, a trough with a 5 m aperture and 7 cm receiver will be expresses as "5 m/7 cm". All other trough configurations will be expressed analogously.

Figure 4 shows plots of intercept factors as a function of incidence angle for select trough configurations for RMS slope errors of 2.5 and 5.4 mrad. The largest incidence angle experienced at Dagget, California, which is the assumed location of the trough field, is 58.2°. The current 5 m/7 cm trough, and the 10 m/14 cm trough have an identical intercept factor that reaches up to 99.6% and decreases to 51.8% at an incidence angle of 58°. A 5 m/14 cm trough is nearly identical. The 10 m/7 cm trough reaches 92.7% and declines steadily to 42% at an incidence angle of 58°. For a larger RMS slope error of 5.4 mrad the 5 m/14 cm trough intercept factor reaches as high as 98.9% and decreases to 51.3% at 58°. The 5 m/7 cm and 10 m/14 cm troughs reach 92.6% and at 58° have an intercept factor 43.3%. The 10 m/7 cm trough has the worst intercept factor; it reaches up to 62.6% and goes down to 27.2% at 58°.

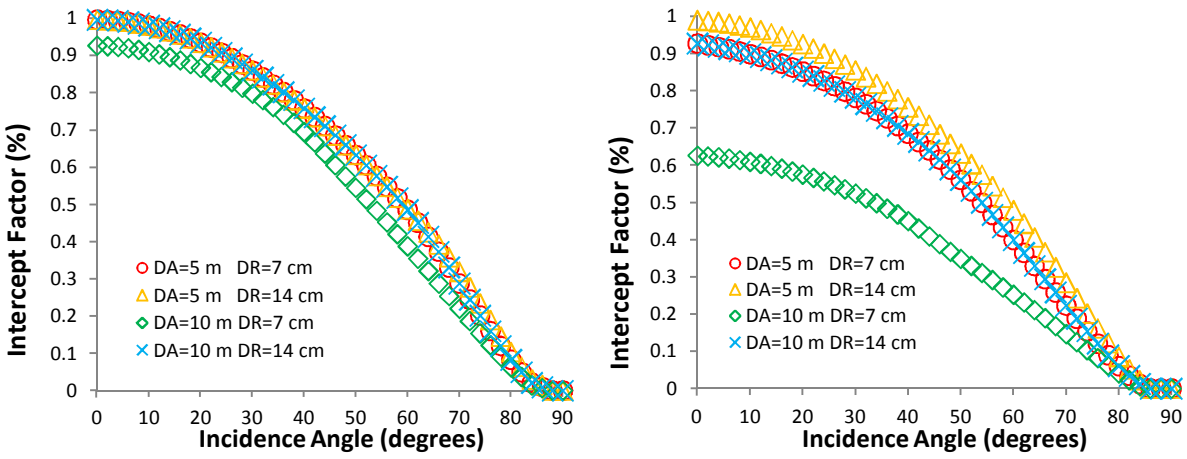

Figure 4. Plot of the intercept factor for selected trough field configurations with an RMS slope error of (left) 2.5 mrad and (right) 5.4 mrad

Figure 5 shows plots of the annual field-wide electrical energy collected for troughs with RMS slope errors of 2.5 mrad and 5.4 mrad. For all the trough configurations considered with an RMS slope error of 2.5 mrad, a 6 m/7 cm trough collected the most energy (116.8 GWh_e) at a loop length of 200 m. A 5 m/14 cm trough collected the least amount of energy because its receiver large convection losses, but at a loop length of 1100 m a 10 m/7 cm trough collected less (110.6 GWh_e). The other configurations shown had roughly the same performance. When the RMS slope error is 5.4 mrad, a 6 m/11.2 cm trough had the best performance at a loop length of 1300 m (113.4 GWh_e). Again the 10 m/ 7 cm trough collected the least amount of energy (89.9 GWh_e) due to its large optical losses. The other configurations had roughly the same performance.

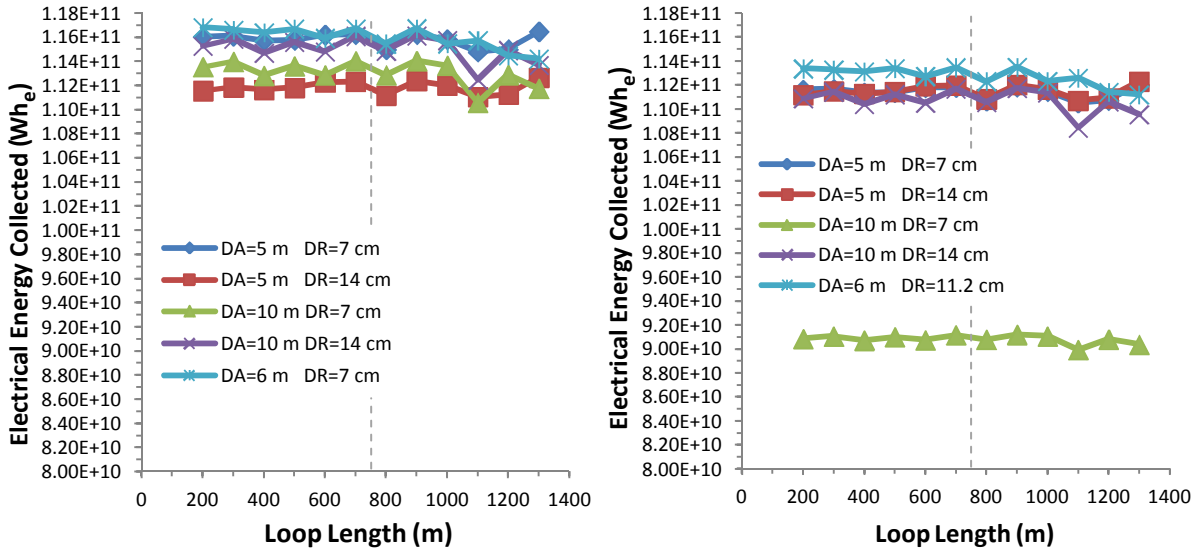

Figure 5. Plot of the field-wide electrical energy collected annually as a function of length for selected trough field configurations with an RMS slope error of (left) 2.5 mrad and (right) 5.4 mrad.

For an RMS slope error of 2.5 mrad a 10 m/ 7 cm trough has a large parasitic pumping power requirement that reaches 27.7 GWh_e at a loop length of 1300 m. A 6 m/7 cm trough had a parasitic pumping power requirement of 10.9 GWh_e with a 5 m/7 cm trough being a little lower at 8.3 GWh_e with the same length. The three trough configurations mentioned have the same receiver tube and show how the parasitic pumping power requirement increases with an increase in aperture size. This because the receiver is subject to more flux per unit length of trough as the aperture size is increased, and as a result the mass flow rate (and consequently the pressure drop) must increase to maintain the trough loop's outlet temperature. When the RMS error is 5.4 mrad the 10 m/7 cm trough has a parasitic power requirement of (18.3 GWh_e). This is smaller than the 2.5 mrad case since less flux reaches the receiver. A 5 m/7 cm trough's parasitics reaches as high as 7.8 GWh_e. All of the remaining selected cases had larger receivers had roughly a 1 GWh_e parasitic pumping power requirement or less. When the loop length is short the number of loops that are required to equal the base case collector area of 188400 m^2 is much larger than for a long loop length. Therefore, for short loop lengths the field-wide mass flow is distributed equally among a greater quantity of loops, decreasing the velocity and loop pressure drop.

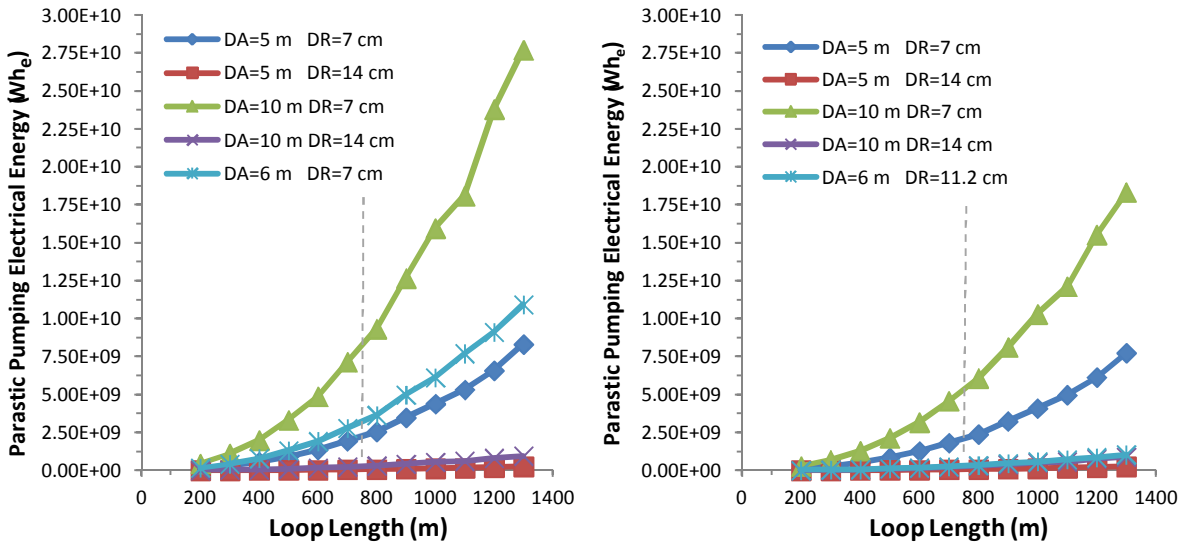

Figure 6. Plot of the field-wide annual parasitic pumping electrical energy requirement as a function of length for selected trough field configurations with an RMS slope error of (left) 2.5 mrad and (right) 5.4 mrad.

Figure 7 is a plot of the annual field-wide electrical energy captured as a function of length after the parasitic pumping electrical energy has been deducted. For an RMS slope error of 2.5 mrad the best performing trough configuration was a 6 m/7 cm trough with a length of 200 m, which collected the most net electrical energy annually (116.6 GWh_e). Troughs with a 10 m/7 cm trough collected at most 113.1 GWh_e at a loop length of 200 m and dropped down to 84.0 GWh_e due to the large parasitic pumping power requirement. For an RMS slope error of 5.4 mrad all trough configurations had roughly the same performance with the exception of the 10 m/ 7cm trough that had dismal performance caused by high optical losses reaching only as high as 90.5 GWh_e at a loop length of 200 and declined to 72.0 GWh_e at 1300 m. The best performing trough was the 6 m/11.2 cm trough at a length of 200 m (113.4 GWh_e). All configurations with a 7 cm receiver were affected by parasitic pumping power as their loop length increased. This effect was smaller for a 5.4 mrad slope error since the flux per unit length and consequently the mass flow rate were smaller.

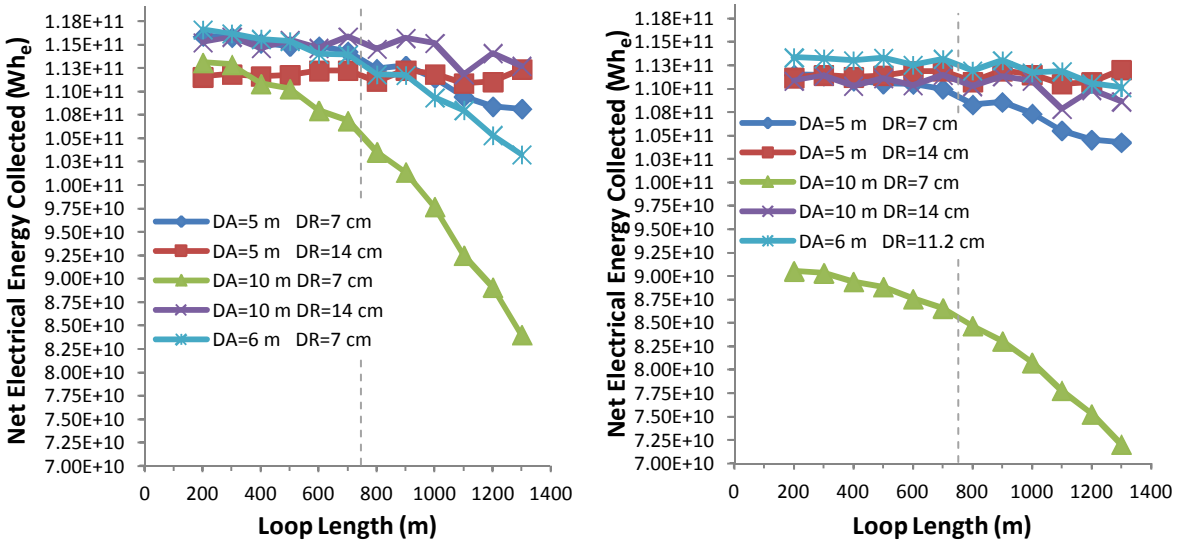

Figure 7. Plot of the field-wide net electrical energy collected annually as a function of length for selected trough field configurations with an RMS slope error of (left) 2.5 mrad and (right) 5.4 mrad.

The following two figures are plots of the net annual field-wide electrical energy captured as a function of aperture size and receiver tube diameter. The data for each aperture and receiver size combination displayed

in these figures are based on the best performing loop lengths for each configuration. The data in Figure 8 is representative of troughs with a 2.5 mrad RMS slope error. The best performing troughs had a 6 m aperture and 7 cm receiver to an 10 m trough with a 11.2 cm receiver (maintaining concentration ratio). While the parasitics for the 5 m/14 cm configuration are small as seen in Figure 7, the larger receiver has a higher convective heat loss, and does not perform as well as the configurations in the range just mentioned. From the base case trough (5 m aperture/7 cm receiver) doubling the aperture to 10 m had a better performance compared to doubling the receiver to 14 cm.

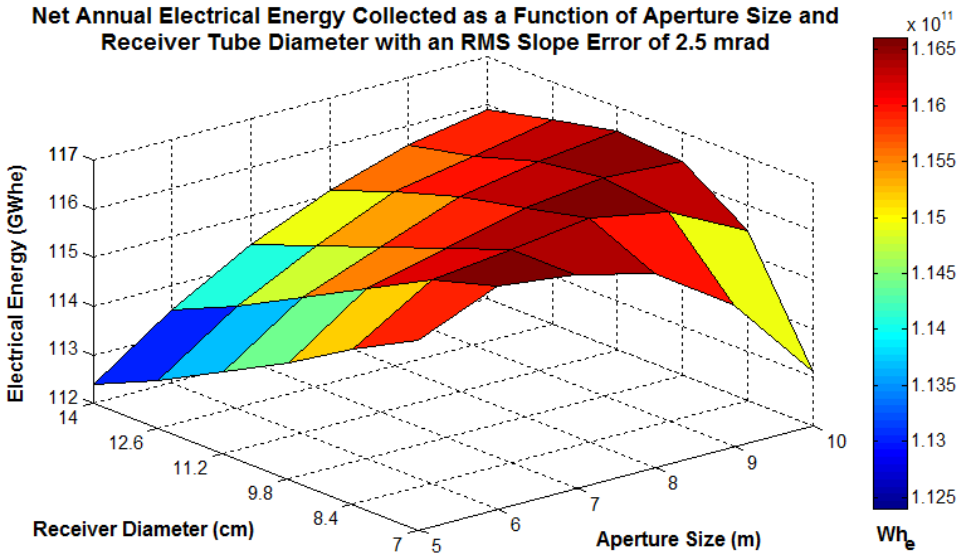

Figure 8. Surface plot of the net annual electrical energy collected as a function of aperture size and receiver tube diameter for a parabolic trough with a 2.5 mrad RMS slope error.

Figure 9 shows the performance of troughs with a 5.4 mrad optical error. Maintaining the concentration ratio yield roughly the same annual performance. Doubling the receiver size from the base case is desirable to doubling the aperture size. The most energy is collected by broadly maintaining the concentration ratio the same as a 5 m/9.8 cm trough. Increasing the concentration ratio beyond the base case trough shows a steady decline to dismal performance at a 10 m/7 cm trough.

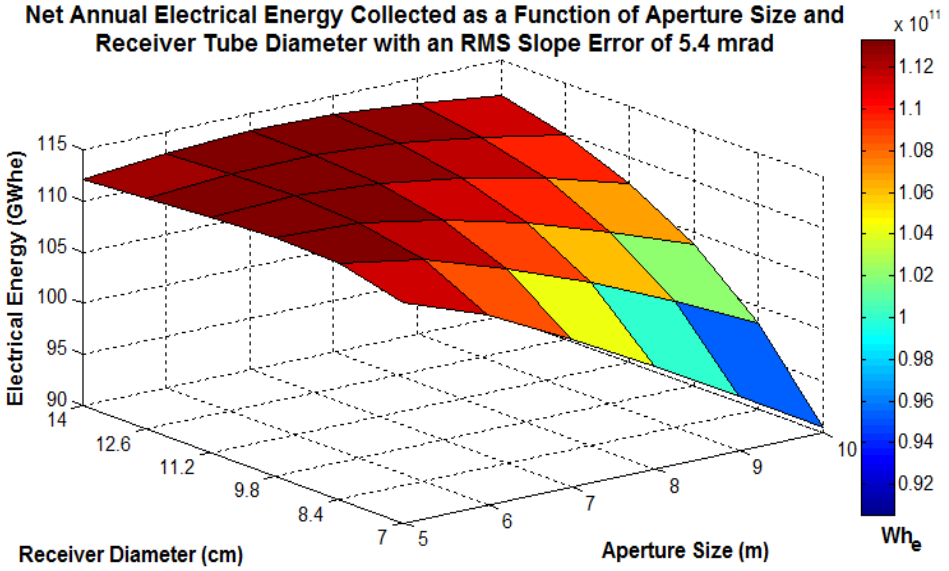

Figure 9. Surface plot of the net annual electrical energy collected as a function of aperture size and receiver tube diameter for a parabolic trough with a 5.4 mrad RMS slope error.

Trough performance is roughly maintained when the concentration ratio is preserved. When the RMS slope error is 5.4 mrad doubling the receiver size from the base case configuration has significantly better performance than doubling the aperture. If gains in optical accuracy can be achieved resulting in an RMS slope error of 2.5 mrad by taking advantage of the suggestions by Kolb and Diver [1], it is better to double the aperture size than to double the receiver size. At this RMS slope error 6 m trough with an 7 cm receiver would collect the most net electrical energy annually 116.6 GWh_e (net). Otherwise, assuming the current slope error budget resulting in a 5.4 mrad RMS slope error, the configuration that collects the most energy annually has a 6 m aperture and 11.2 cm receiver (113.4 GWh_e).

Acknowledgments: Sandia National Laboratories is a multi-program laboratory managed and operated by Sandia Corporation, a wholly owned subsidiary of Lockheed Martin Corporation, for the U.S. Department of Energy's National Nuclear Security Administration under contract DE-AC04-94AL85000.

References

[1] Diver, G.J., & Kolb, R.B, 2011, "Conceptual Design of a 2x Trough for Use Within Salt and Oil-Based Parabolic Trough Power Plants", Journal of Solar Energy Engineering, Vol. 132.

[2] Glenn, K.W., C.K., Ho, G.J., Kolb, 2011, "Parametric Analysis of Parasitic Pressure Drop and Heat Losses for a Parabolic Trough with Considerations of Varying Aperture Sizes and Receiver Sizes", in proceedings of the 2011 ASME Energy Sustainability Conference, Washington D.C., August 7-10, 2011.

[3] Luz Engineering Corporation, 1989, "Luz Engineering Corporation SEGS VI & VII Operations Manual".

[4] National Renewable Energy Laboratory, 1995, *National Solar Radiation Database* [23161.tm2], Retrieved from http://rredc.nrel.gov/solar/old_data/nsrdb/1961-1990/tmy2/

[5] Rabl, A, & Bendt, P, 1982, Effect of Circumsolar Radiation on Performance of Focusing Collectors, Journal of Solar Energy Engineering, Vol. 104, 237-250.

[6] King, D.L., 1982. Beam Quality and Tracking Accuracy Evaluation of Second-Generation and Barstow Production Heliostats. SAND82-0181, Albuquerque, NM: Sandia National Laboratories

[7] National Renewable Energy Laboratory, 2012, SolTrace (Version 2012.3.28) [Software], Available from http://www.nrel.gov/csp/soltrace/download.html

[8] Forristall, R., 2003, "Heat Transfer Analysis and Modeling of a Parabolic Trough Solar Receiver Implemented in Engineering Equation Solver", NREL Contract No. DE-AC36-99-GO10337, Golden, CO: National Renewable Energy Laboratory

[9] Deutsche Forschungsanstalt für Luft- und Raumfahrt e.V., 1993, *Second Generation Central Receiver Technologies: A Status Report* (Becker & Klimas, Eds.). Karlsruhe, Germany: C.F. Müller.

[10] National Oceanic & Atmoshperic Association's Earth System Research Laboratory, 2011, Solar Position Calculator. http://www.srrb.noaa.gov/highlights/sunrise/azel.html